Quantum state synthesis of superconducting resonators

Roshan Sharma and Frederick W. Strauch*
Williams College, Williamstown, Massachusetts 01267, USA
(Received 13 March 2015; revised manuscript received 30 July 2015; published 26 January 2016)

We present a theoretical analysis of different methods to synthesize entangled states of two quantum mechanical resonators. These methods are inspired by experimentally demonstrated interactions of superconducting resonators with artificial atoms, and offer efficient routes to generate nonclassical states. Using a two-mode Jaynes-Cummings model, we analyze the theoretical structure of these algorithms and their average performance for arbitrary states and for deterministically preparing NOON and maximally entangled states. Using a new state synthesis algorithm, we show that NOON and maximally entangled states can be prepared in a time linear in the desired photon number and without any state-selective interactions.

DOI: 10.1103/PhysRevA.93.012342

I. INTRODUCTION

In recent years we have witnessed a dramatic evolution in the quantum mechanical experiments performed with superconducting circuits. Initially, the challenge was to fabricate, prepare, and isolate signatures of quantum behavior of the coupled motion of Cooper pairs through Josephson junctions and electrodynamic oscillations in superconducting devices [1–4]. This has now become routine in the field of circuit quantum electrodynamics (QED) [5], and the frontier is designing and manipulating the quantum states of coupled superconducting qubits (quantum bits) and resonators to achieve quantum-enhanced information processing [6,7].

When embarking on this new journey, the quantum mechanical engineer must decide on which degrees of freedom she wishes to manipulate: the electronic (qubit) or electromagnetic (resonator)? There are important advantages on both sides, but, until recently [8], the coherence (or quality factor) of superconducting resonators (or cavities) could be significantly greater than the qubit circuits utilizing Josephson junctions. Thus, one should consider what coherent operations can be performed with superconducting resonators as opposed to qubit circuits. Such studies include high-fidelity measurement [9,10], computation [11], and error correction [12,13], which all attempt to utilize the larger state space afforded by the harmonic oscillator states of a resonator to achieve greater efficiency.

There are many other systems in nature which have harmonic oscillator modes that can be accessed at the quantum level. These include the photon states in cavity QED, which can be selectively excited by laser-controlled atoms, or the motional states of trapped ions when driven by sideband transitions [14]. The collective quantum states of atomic or spin ensembles also have harmonic oscillator modes that could be controlled [15,16]. Finally, mechanical oscillators can be prepared and manipulated at the quantum level [17,18]. For all of these systems, a theoretical understanding of methods to manipulate their quantum states is an important topic.

In this paper, we consider how to perform "digital" state synthesis of superconducting resonators, where the desired state is a superposition of Fock states [19,20]. In particular, we continue the development of theoretical methods [21–24] to synthesize an entangled superposition of the Fock states between two resonators. This complements the many recent studies [11,25–28] of how to perform quantum computation using such systems as qudits [29], in which d levels are used as a quantum digit. An alternative "analog" approach uses superpositions of coherent states to store quantum information [30]. We expect that many of the issues encountered in the digital regime will have counterparts in the analog regime, but both warrant detailed study. Finally, we note that there have been a number of other studies of interesting interactions that can be used to generate entanglement between superconducting or nanomechanical resonators [31–35]. While our results are primarily theoretical, we expect that the methods and ideas presented here will inform the control of these and other quantum oscillators.

The general state synthesis problem concerns how one can prepare, with high fidelity, an arbitrarily chosen quantum state. A *state synthesis algorithm* is a procedure, given a description of the target state, to identify the appropriate set of Hamiltonian controls (such as amplitudes and frequencies of control fields) that will prepare the target state from a fixed initial state. Note that there are two senses in which the state synthesis problem is solved algorithmically. First, the algorithm is typically implemented as a computer program and run on classical hardware. Second, the output of this program is a list of operations to be applied to quantum hardware to prepare the desired state. Thus, the state synthesis algorithms presented here can be used to program future quantum machines.

In this paper we consider scenarios such as those depicted in Fig. 1, in which a qubit is used to couple two resonant cavities A and B, the latter with Fock states $|n_a\rangle \otimes |n_b\rangle$. We will analyze algorithms that deterministically and exactly produce an arbitrarily chosen state of two resonators, of the form,

$$|\psi_{\text{target}}\rangle = |0\rangle_{\text{qubit}} \otimes \sum_{n_a=0}^{N_a} \sum_{n_b=0}^{N_b} c_{n_a,n_b} |n_a\rangle \otimes |n_b\rangle. \qquad (1)$$

In fact, we will provide a detailed performance analysis of two such algorithms, one a "photon subtraction" algorithm based on previous work [21,36], and a second "photon swapping" algorithm new to this work. In the spirit of Law and Eberly's classic study of controlling a qubit-resonator system [37], we explore a simplified model of two resonators coupled to

*frederick.w.strauch@williams.edu

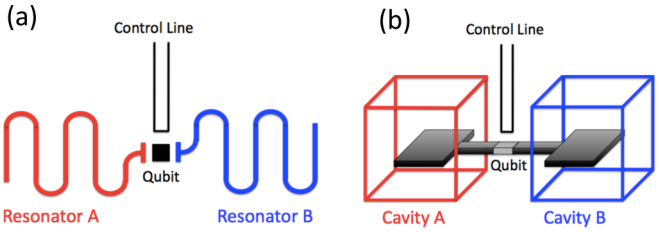

FIG. 1. Schematic scenario for entangled state synthesis problems, in which two cavities A and B are coupled by a qubit, using (a) a planar coplanar waveguide circuit, or (b) two three-dimensional cavities. The qubit can be controlled to effect qubit rotations or swaps between the qubit and each cavity.

a qubit, here called the driven two-mode Jaynes-Cummings Hamiltonian:

$$\mathcal{H}/\hbar = \omega_a a^\dagger a + \omega_b b^\dagger b + \omega_q(t)\sigma^\dagger\sigma + F(t)\sigma_x + g_a(t)(\sigma^\dagger a + \sigma a^\dagger) + g_b(t)(\sigma^\dagger b + \sigma b^\dagger). \quad (2)$$

Here a, b, and $\sigma = |0\rangle\langle 1|$ are the annihiliation operators for the two resonators and qubit, respectively, and $\sigma_x = \sigma + \sigma^\dagger$. The resonator frequencies are ω_a and ω_b, while the qubit frequency $\omega_q(t)$, the driving field $F(t)$, and the couplings $g_a(t)$ and $g_b(t)$ are all treated as possible control parameters. By turning these parameters on and off according to the state synthesis algorithm, one can evolve the initial ground state $|0\rangle_{\text{qubit}} \otimes |0\rangle \otimes |0\rangle$ to the desired target state $|\psi_{\text{target}}\rangle$.

While our state synthesis algorithms are based on the above model, implementing the algorithms using a specific Hamiltonian appropriate to experimental implementations in circuit QED, and the expected fidelity in the presence of decoherence, have been discussed in previous work [36]. In this context, it is important to note that time-dependent control of the qubit frequency $\omega_q(t)$ and driving field $F(t)$ was used to experimentally synthesize Fock states and their superpositions in a single coplanar waveguide resonator using a phase qubit [19,20]. This approach was extended to a system similar to that in Fig. 1(a) and used to controllably swap excitations between [7] and to prepare entangled states of two resonators [38]. However, it was argued [21] that, for an *arbitrary* target state, the algorithm must use state-selective interactions, such as the number-state-dependent qubit transitions found in experiments with a transmon qubit coupled to a resonator [39–43]. Although these experiments involved planar circuits, there also has been significant progress toward tunable devices coupled to three-dimensional cavities [44,45]. Furthermore, while the state-synthesis algorithms discussed here can be adapted to systems with fixed couplings, our final results may be most relevant for systems with controllable couplings. Controllable couplings between qubits and resonators [46–49], between high-coherence qubits [50], and between planar [51] and three-dimensional [52] cavities have also been experimentally demonstrated. This last experiment used a system very similar to that in Fig. 1(b).

The results obtained here can be used both as a guide to future experiments using advanced circuit QED circuits, and as a theoretical benchmark for alternative procedures to prepare such states. These alternatives include using other interactions (such as sideband transitions [53–55]), numerical optimization methods [56], closed-loop control [57], or other measurement-based methods for state preparation [58]. In this work, we will identify how physical resources, such as the number and type of controls and the average time required, scale with the size of the desired target state. In particular, we apply our new algorithm to NOON-state preparation, for which a special-purpose algorithm using a multilevel device [22] was previously demonstrated [38]. We go beyond our previous work [21,36] to find that our new algorithm can synthesize the following class of entangled states (with $N_a = N_b = N$) in a time *linear* in the state size and *without* state-selective interactions:

$$|\psi_{\text{target}}\rangle = |0\rangle_{\text{qubit}} \otimes \sum_{n=0}^{N} c_n |n\rangle \otimes |N-n\rangle. \quad (3)$$

As state-selective interactions are often weaker than direct qubit-resonator interactions [9,26], we expect these results will aid future demonstrations of entanglement in superconducting or other qubit-resonator systems.

This paper is organized as follows. In Sec. II, we introduce the general state synthesis problem by studying how to prepare a general state of a d-level quantum system (i.e., a qudit). This is followed in Sec. III by a presentation of the Law-Eberly algorithm for a single resonator coupled to a qubit, before addressing in Sec. IV the two entangled-state synthesis algorithms for two resonators coupled by a qubit. Finally, Sec. V compares these algorithms for the preparation of NOON and maximally entangled states. We conclude in Sec. VI by summarizing our work and open questions. The appendix details how to generate the appropriate interactions from the driven two-mode Jaynes-Cummings Hamiltonian.

II. QUDIT STATE SYNTHESIS

Before focusing on state synthesis problems for qubit-resonator systems, it is useful to start with a simpler problem. Thus, we begin by considering the synthesis of an arbitrary state of a d-level system known as a qudit (a quantum digit) [29]. Such systems are universal for computation [59,60], and much is known about the construction of logic operations [61–64] and error correcting codes [29,65] using such systems. A superconducting qudit could be a nonlinear oscillator driven directly by control fields with frequencies tuned to distinct transitions (as in the phase qudit experiment [66]), or a driven qubit-resonator system with either resonant or dispersive coupling to a qubit [26].

Our task is to prepare the quantum state,

$$|\psi_{\text{target}}\rangle = \sum_{n=0}^{d-1} c_n |n\rangle, \quad (4)$$

starting from the initial state $|0\rangle$. For ease of analysis, we write the coefficients of the target state $|\psi\rangle$ in terms of d phases and d-dimensional spherical polar coordinates,

$$c_0 = \cos\theta_0 e^{i\phi_0},$$
$$c_1 = \sin\theta_0 \cos\theta_1 e^{i\phi_1},$$
$$\vdots$$

$$c_{d-2} = \sin\theta_0 \sin\theta_1 \cdots \sin\theta_{d-3} \cos\theta_{d-2} e^{i\phi_{d-2}},$$
$$c_{d-1} = \sin\theta_0 \sin\theta_1 \cdots \sin\theta_{d-3} \sin\theta_{d-2} e^{i\phi_{d-1}}, \quad (5)$$

where the angles have the ranges $0 \leqslant \theta_j \leqslant \pi/2$ and $-\pi < \phi_j \leqslant \pi$. Note that the first phase ϕ_0 could be set to zero without changing the physical problem.

The quantum state can be generated by two natural single-qudit operations: the two-level rotations,

$$\mathcal{R}_{n,n+1}(\theta) = \exp\left[-i\frac{\theta}{2}(|n\rangle\langle n+1| + |n+1\rangle\langle n|)\right], \quad (6)$$

and the single-level phase shifts,

$$\mathcal{Z}_n(\phi) = \exp(i\phi|n\rangle\langle n|). \quad (7)$$

In terms of these operations, a solution to the state synthesis problem is the following:

$$|\psi\rangle = \mathcal{Z}_{d-1}(\phi_{d-1})\left(\prod_{k=0}^{d-2} \mathcal{Z}_k(\phi_k)\mathcal{Z}_{k+1}(\pi/2)\mathcal{R}_{k,k+1}(2\theta_k)\right)|0\rangle, \quad (8)$$

where we are using a "time-ordered" product notation, e.g.,

$$\prod_{j=1}^{d-1} U_j = U_{d-1}U_{d-2}\cdots U_1. \quad (9)$$

For a qubit ($d = 2$), this reduces to $\mathcal{Z}_0(\phi_0)\mathcal{Z}_1(\phi_1 + \pi/2)\mathcal{R}_{0,1}(2\theta_0)$, which can be combined into the product of two spin rotations (about the x and z axes, respectively). This is the number of rotations required to map an arbitrary qubit state's Bloch vector from the north pole to any point on the Bloch sphere. Similarly, this solution is a minimal approach to controlling a qudit, using a fixed set of operations for an arbitrary state of the form Eq. (4).

While this solution can be verified by inspection, an alternative approach, the prototype for the state synthesis algorithms to be described below, is to find the rotations by reversing the time evolution, that is, to choose a set of operations $U_j^\dagger$ such that

$$\prod_{j=d-1}^{1} U_j^\dagger|\psi\rangle = U_1^\dagger \cdots U_{d-1}^\dagger|\psi\rangle = |0\rangle. \quad (10)$$

By simple inversion of this sequence of operations, we can use this solution to the inverse evolution equation to find a solution of the state synthesis problem given by Eq. (8). The algorithmic approach is to choose each operation to "zero out" an amplitude of the target state. Once all of the amplitudes have been removed, save that for state $|0\rangle$, a solution to Eq. (10) is obtained. To see this in more detail, we index the steps of the algorithm and define the quantum state,

$$|\psi_j\rangle = U_j^\dagger|\psi_{j+1}\rangle, \quad (11)$$

where $|\psi_d\rangle = |\psi\rangle$ and $j = d-1 \to 0$. The operator $U_j^\dagger$ is then chosen to remove the corresponding state amplitude, so that

$$\langle j|\psi_j\rangle = 0. \quad (12)$$

Using the rotations specified above, we can set

$$U_j^\dagger = \mathcal{R}_{j-1,j}^\dagger(\gamma_j)\mathcal{Z}_j^\dagger(\beta_j)\mathcal{Z}_{j-1}^\dagger(\alpha_j). \quad (13)$$

The amplitude in Eq. (12) is then "zeroed" with the solution,

$$\alpha_j = \arg(\langle j-1|\psi_{j+1}\rangle),$$
$$\beta_j = \frac{\pi}{2} + \arg(\langle j|\psi_{j+1}\rangle), \quad (14)$$
$$\gamma_j = 2\arctan\left(\left|\frac{\langle j|\psi_{j+1}\rangle}{\langle j-1|\psi_{j+1}\rangle}\right|\right).$$

Before verifying that this produces the same solution as Eq. (8), let us consider the first rotation $U_{d-1}^\dagger$ in Eq. (10) (the last rotation of the forward sequence). This is chosen to remove the highest state $|d-1\rangle$ from the superposition in $|\psi_d\rangle$. Using Eqs. (4) and (13) we have

$$\langle d-1|U_{d-1}^\dagger|\psi\rangle = e^{-i\beta_{d-1}}\cos(\gamma_{d-1}/2)c_{d-1} + ie^{-i\alpha_{d-1}}\sin(\gamma_{d-1}/2)c_{d-2}. \quad (15)$$

Using the spherical coordinates for c_{d-2} and c_{d-1} from Eq. (5) (and canceling common terms), we thus require

$$\cos(\gamma_{d-1}/2)\sin\theta_{d-2}e^{-i\beta_{d-1}}e^{i\phi_{d-1}} + i\sin(\gamma_{d-1}/2)\cos\theta_{d-2}e^{-i\alpha_{d-1}}e^{i\phi_{d-2}} = 0, \quad (16)$$

which is satisfied by

$$\alpha_{d-1} = \phi_{d-2},$$
$$\beta_{d-1} = \frac{\pi}{2} + \phi_{d-1}, \quad (17)$$
$$\gamma_{d-1} = 2\theta_{d-2},$$

in complete agreement with Eq. (14).

The same procedure works for each $U_j^\dagger$. However, the choice of α_j ensures that the phase of $\langle j|\psi_{j+1}\rangle$ is zero, for each $j = d-2, d-3, \ldots$, so that in general we find

$$\alpha_j = \phi_{j-1},$$
$$\beta_j = \frac{\pi}{2} + \delta_{j,d-1}\phi_j, \quad (18)$$
$$\gamma_j = 2\theta_{j-1}.$$

Using these angles, we see that

$$|\psi\rangle = \prod_{j=1}^{d-1} U_j|0\rangle = U_{d-1}\cdots U_1|0\rangle, \quad (19)$$

with

$$U_j = \mathcal{Z}_{j-1}(\alpha_j)\mathcal{Z}_j(\beta_j)\mathcal{R}_{j-1,j}(\gamma_j), \quad (20)$$

agrees with Eq. (8) after setting $k = j-1$. Note, however, that the choice of the angles is not unique. We could have set $\alpha_j = 0$ and $\beta_j = \pi/2 + (\phi_j - \phi_{j-1})$ to achieve the same result.

For an arbitrary target state $|\psi\rangle$, we can characterize the performance of this algorithm in terms of the resources needed to construct the state. These resources could be analyzed in terms of the number of controls required, the energy associated with each control, and the duration over which the control fields act. While the exact resources will depend on the actual

details of an experimental implementation, we can use our algorithm to estimate the overall time required in the following way. We postulate that each of the two-state rotations occurs with an effective Rabi frequency Ω and each phase shift with $\pm\Delta\omega$. Then, this algorithm produces a set of $d-1$ phase shifts (assuming α and β can occur in parallel) and $d-1$ rotations, such that the overall time is

$$T = \frac{1}{\Delta\omega}\sum_{j=1}^{d-1}|\beta_j| + \frac{1}{\Omega}\sum_{j=1}^{d-1}\gamma_j. \tag{21}$$

The average time required can be found by averaging over the unit circle (for β_j) and the spherical coordinates in Eq. (5) (for $\gamma_j = 2\theta_j$). We find that $\langle|\beta_j|\rangle = \pi/2$ and

$$\langle\theta_j\rangle = \frac{\int_0^{\pi/2}\theta(\sin\theta)^{d-2-j}d\theta}{\int_0^{\pi/2}(\sin\theta)^{d-2-j}d\theta} \approx \frac{\pi}{2} - \frac{\pi}{4}\frac{1}{\sqrt{d-2-j}}. \tag{22}$$

Thus, we find that

$$\langle T\rangle = \left(\frac{\pi}{\Omega} + \frac{\pi}{2\Delta\omega}\right)(d-1) - \frac{\pi}{2\Omega}\sum_{k=1}^{d-1}\frac{1}{\sqrt{k}}. \tag{23}$$

Thus, this particular sequence takes a time that grows roughly linear in the Hilbert space dimension d, with time scales given by $1/\Omega$ and $1/\Delta\omega$. For the state-synthesis algorithms to be presented below, our goal will be to find how the resources scale, on average, with the Hilbert space dimension.

III. LAW-EBERLY ALGORITHM

Having illustrated the properties of qudit state synthesis, we proceed to a qubit-oscillator system, appropriate for superconducting circuits and resonators. This algorithm was first put forward by Law and Eberly in the context of cavity QED [37], and experimentally demonstrated using the internal and vibrational states of a trapped ion [67]. The superconducting experiments [19,20], using this algorithm, demonstrated exquisite control over the combined Hilbert space of the qubit-resonator system. For completeness, and to better understand the two-resonator constructions to be presented below, we review this problem.

The goal of the Law-Eberly algorithm is to synthesize an arbitrary state of harmonic oscillator mode (the resonator) by using a two-level auxiliary system (qubit). The target state is taken to be

$$|\psi_{\text{target}}\rangle = |0\rangle\otimes\sum_{n=0}^{N_{\max}} c_n|n\rangle, \tag{24}$$

in which the resonator has a maximum photon number $N_{\max}$. The system is modeled by a Hamiltonian of the Jaynes-Cummings type [68], with a Hamiltonian (in the interaction picture) of the form,

$$\mathcal{H}/\hbar = \Delta\omega(t)\sigma^\dagger\sigma + \tfrac{1}{2}\Omega(t)\sigma_x + g(t)(\sigma^\dagger a + \sigma a^\dagger), \tag{25}$$

where $\sigma = |0\rangle\langle 1|$ is the lowering operator for the qubit and the control fields $\Delta\omega(t)$, $\Omega(t)$, and $g(t)$ can be turned on and off to achieve the operations above. This formulation is natural in the cavity QED context, and can be applied to circuit QED [20] with minor modifications. Our goal is to characterize the performance of this algorithm, using the average resources needed to prepare an arbitrary target state.

Using the Hamiltonian Eq. (25), one can implement the unitary operations,

$$S(\theta) = \exp[-i\theta(a\sigma^\dagger + a^\dagger\sigma)], \tag{26}$$

$$R(\theta) = \exp\left(-i\frac{\theta}{2}\sigma_x\right), \tag{27}$$

and

$$Z(\phi) = \exp\left(-i\frac{\phi}{2}\sigma_z\right), \tag{28}$$

by turning on (and off) the controls $g(t)$, $\Omega(t)$, and $\Delta\omega(t)$, respectively. The Law-Eberly algorithm will be expressed in terms of these operations.

The state-synthesis procedure follows a similar pattern as the qudit case presented above. We first set

$$|\psi_j\rangle = U_j^\dagger|\psi_{j+1}\rangle, \tag{29}$$

where

$$U_j^\dagger = R^\dagger(\gamma_j)Z^\dagger(\beta_j)S^\dagger(\theta_j)Z^\dagger(\alpha_j), \tag{30}$$

and $|\psi_{N+1}\rangle = |\psi_{\text{target}}\rangle$. Here α,β,γ, and θ are chosen so that at each step,

$$\langle 0,j|\psi_j\rangle = \langle 1,j|\psi_j\rangle = 0. \tag{31}$$

These angles are then found for each $j = N \to 1$, after which $|\psi_1\rangle = |0,0\rangle$. The inverse sequence specifies how to prepare the target state using only qubit rotations, phase shifts, or qubit-resonator swaps.

To see how this can be accomplished, it is convenient to break Eq. (29) into two steps by defining

$$|\psi_{j+1/2}\rangle = S^\dagger(\theta_j)Z^\dagger(\alpha_j)|\psi_{j+1}\rangle, \tag{32}$$

and

$$|\psi_j\rangle = R^\dagger(\gamma_j)Z^\dagger(\beta_j)|\psi_{j+1/2}\rangle. \tag{33}$$

In addition, we define

$$\psi_{q,k}(j) = \langle q,k|\psi_j\rangle, \text{ where } q = 0 \text{ or } 1. \tag{34}$$

The first step of the algorithm (for the inverse evolution) solves $\psi_{0,j}(j+1/2) = 0$. Using Eq. (32), this reduces to

$$e^{i\alpha_j/2}\cos(\sqrt{j}\theta_j)\psi_{0,j}(j+1) + ie^{-i\alpha_j/2} \times \sin(\sqrt{j}\theta_j)\psi_{1,j-1}(j+1) = 0, \tag{35}$$

or

$$e^{-i\alpha_j}\tan(\sqrt{j}\theta_j) = i\frac{\psi_{0,j}(j+1)}{\psi_{1,j-1}(j+1)}. \tag{36}$$

This has the solution,

$$\alpha_j = \arg\left(\frac{\langle 1,j-1|\psi_{j+1}\rangle}{i\langle 0,j|\psi_{j+1}\rangle}\right), \qquad \theta_j = \frac{1}{\sqrt{j}}\arctan\left(\left|\frac{\langle 0,j|\psi_{j+1}\rangle}{\langle 1,j-1|\psi_{j+1}\rangle}\right|\right). \tag{37}$$

The second step solves $\psi_{1,j-1}(j) = 0$. Using Eq. (33), this reduces to

$$e^{-i\beta_j/2}\cos\left(\frac{\gamma_j}{2}\right)\psi_{1,j-1}(j+1/2) + ie^{i\beta_j/2}\sin\left(\frac{\gamma_j}{2}\right)\psi_{0,j-1}(j+1/2) = 0, \quad (38)$$

or

$$e^{i\beta_j}\tan\left(\frac{\gamma_j}{2}\right) = i\frac{\psi_{1,j-1}(j+1/2)}{\psi_{0,j-1}(j+1/2)}. \quad (39)$$

This, in turn, has the solution,

$$\beta_j = \arg\left(\frac{i\langle 1,j-1|\psi_{j+1/2}\rangle}{\langle 0,j-1|\psi_{j+1/2}\rangle}\right), \qquad \gamma_j = 2\arctan\left(\left|\frac{\langle 1,j-1|\psi_{j+1/2}\rangle}{\langle 0,j-1|\psi_{j+1/2}\rangle}\right|\right). \quad (40)$$

By solving these equations for $\alpha_j, \beta_j, \gamma_j$, and θ_j for $j = N \to 0$, keeping track of $|\psi_j\rangle$ at each step, the amplitude is forced down to smaller and smaller photon numbers, so that $|\psi_0\rangle = |0,0\rangle$. The form of the sequence was chosen specifically to not send amplitude to higher photon numbers. That is, the algorithm actually produces operators U_j and states $|\psi_j\rangle$ that satisfy the condition,

$$\langle 0,k|\psi_j\rangle = \langle 1,k|\psi_j\rangle = 0 \text{ for } k \geqslant j. \quad (41)$$

Satisfying this condition for two or more resonators is the greatest challenge for generalizations of the Law-Eberly algorithm. In the two-resonator case, to be considered shortly, the algorithm must simultaneously ensure that amplitude is not sent to higher photon numbers for either resonator mode.

The average values of $\alpha_j, \beta_j, \gamma_j$, and θ_j can be used to find the average time required, assuming constant controls $\pm\Delta\omega$, Ω, and g:

$$T = \frac{1}{\Delta\omega}\sum_{j=1}^{N\max}(|\alpha_j| + |\beta_j|) + \frac{1}{\Omega}\sum_{j=1}^{N\max}\gamma_j + \frac{1}{g}\sum_{j=1}^{N\max}\theta_j. \quad (42)$$

We illustrate the average angles obtained with Eqs. (37) and (40) in Fig. 2. Here we have generated 100 random target states for each value of $N_{\max}$ and averaged the total of the angles used in the Law-Eberly algorithm. Also shown are the approximations,

$$\sum_j\langle|\alpha_j| + |\beta_j|\rangle \approx \pi\left(N_{\max} - \frac{1}{2}\right), \qquad \sum_j\langle\gamma_j\rangle \approx 2.72N_{\max} - 1.66, \qquad \sum_j\langle\theta_j\rangle \approx 2.65\sqrt{N_{\max}} - 1.78, \quad (43)$$

obtained by fitting the numerical data.

The linear increase of the phases and qubit rotations are expected, as each step requires such a rotation, while the square-root dependence of $\sum_j\langle\theta_j\rangle$ is due to the $\sqrt{n}$ coupling between the qubit and the n-photon state of the resonator. When these averaged angles are substituted into Eq. (42), we see that, just as the qudit case, an arbitrary state of the form Eq. (24) can be synthesized in a time proportional to the effective Hilbert-space dimension.

IV. TWO-RESONATOR ALGORITHMS

The state synthesis problem can be extended to any number of resonators, but explicit algorithms are a challenge to specify. Early work utilized special interactions [69–73] to enable the transfer of excitations between resonators and multilevel atoms. These interactions, while possible for trapped-ion systems, are harder to realize in other resonator systems. As we are interested in Fock-state control, we restrict our attention to the simplest system of a single qubit coupling two resonators, with the general target state,

$$|\psi_{\text{target}}\rangle = |0\rangle\otimes\sum_{n_a=0}^{N_a}\sum_{n_b=0}^{N_b}c_{n_a,n_b}|n_a\rangle\otimes|n_b\rangle. \quad (44)$$

In general, such a state will be entangled, thus we call this the entangled-state synthesis problem. To analyze the state-synthesis algorithms, we use a simplified form of the two-mode driven Jaynes-Cummings Hamiltonian:

$$\mathcal{H}/\hbar = \Delta\omega(t)\sigma^\dagger\sigma + \frac{1}{2}\sum_{n_a,n_b}\Pi_{n_a,n_b}\Omega_{n_a,n_b}(t)\sigma_x + g_a(t)(\sigma^\dagger a + \sigma a^\dagger) + g_b(t)(\sigma^\dagger b + \sigma b^\dagger), \quad (45)$$

where the control fields $\Delta\omega(t)$, $\Omega_{n_a,n_b}(t)$, $g_a(t)$, and $g_b(t)$ can be turned on and off at will, and where we have defined a set

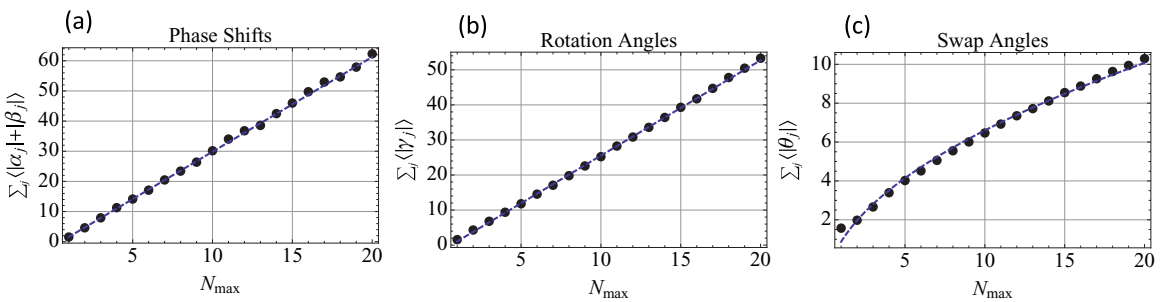

FIG. 2. Averaged total angles for the state synthesis sequence using the Law-Eberly algorithm.

of projection operators,

$$\Pi_{n_a,n_b} = |n_a,n_b\rangle\langle n_a,n_b|. \tag{46}$$

The physics underlying this projection operator is due to Stark shift of the qubit in the dispersive regime of the underlying Jaynes-Cummings Hamiltonian. These Stark shifts allow for a number-state selective Rabi rotation of the qubit. Such selective operations were first observed in circuit QED as number splitting [39] and later used for photon measurement [42] and theoretically proposed for entangled-state synthesis [21]. A derivation of this effective Hamiltonian from the original driven two-mode Jaynes-Cummings model is presented in the appendix.

Using this effective Hamiltonian, steps of the algorithm will involve the swap operators,

$$\begin{aligned} A(\theta) &= \exp[-i\theta(a\sigma^\dagger + a^\dagger\sigma)], \\ B(\theta) &= \exp[-i\theta(b\sigma^\dagger + b^\dagger\sigma)], \end{aligned} \tag{47}$$

the single-qubit phase rotations,

$$Z(\phi) = \exp\left(-i\frac{\phi}{2}\sigma_z\right), \tag{48}$$

and the number-state-selective qubit rotations,

$$R_{n_a,n_b}(\theta) = \exp\left(-i\frac{\theta}{2}\sigma_x \otimes |n_a,n_b\rangle\langle n_a,n_b|\right). \tag{49}$$

The first three operators correspond to turning on (and off) the controls g_a, g_b, and $\Delta\omega$, respectively. The last operation corresponds to a special application of the Rabi control $\Omega(t)$ to drive a state-selective Rabi transition, for state $|n_a,n_b\rangle$ only. We note that this last condition is not necessary, as the state synthesis algorithms can be performed with reduced selectivity [21,36]. In fact, we will discuss applications that require no selectivity at all in the following section.

To analyze the algorithms, we use a Fock-state diagram, such as Fig. 3, in which a state $|n_a,n_b,q\rangle$ with n_a excitations in mode A, n_b excitations in mode B, and qubit state q is indicated by the node at location (n_a,n_b) and internal level q. Each of the operations described above corresponds to a transition between sets of states in this diagram, and the state synthesis sequence can be interpreted using paths in this diagram. Two algorithms, to be described below, can be visualized using these diagrams. The first algorithm, shown in Fig. 3(a), which we call the photon subtraction algorithm, uses vertical and horizontal paths from top to bottom and left to right in the Fock-state diagram. The second algorithm, shown in Fig. 3(b) which we call the photon swapping algorithm, uses diagonal paths from the upper left to the lower right. These are the two natural choices for how to navigate the Fock-state diagram in order to program the quantum system into any desired state. In this section, we will analyze each algorithm in detail, and compare their average performance when preparing an arbitrary two-resonator state of the form Eq. (44).

A. Algorithm 1: Photon subtraction

The first algorithm for superconducting resonators [21] used a strategy similar to the trapped-ion proposal by Kneer and Law [72], and involves repeated subtraction of photons from one of the resonators. In terms of the Fock-state diagram presented, state amplitudes are cleared column-by-column, row-by-row, until all of the remaining photons are in one mode only. The final steps remove these photons by the Law-Eberly protocol described above.

The essential steps can be written as

$$U = \left(\prod_{j=1}^{N_b} U_{b,j}\right) U_a, \tag{50}$$

where

$$U_a = \prod_{j=1}^{N_a} Z(\alpha_j)A(\theta_j)Z(\beta_j)R(\gamma_j), \tag{51}$$

and

$$U_{b,j} = \prod_{k=0}^{N_b} Z(\alpha_{jk})B(\theta_{jk})Z(\beta_{jk})R_{n_a=k}(\gamma_{jk}). \tag{52}$$

Read in reverse, the elements of U_a and $U_{b,j}$ are all of the form of Eq. (30), with phases and angles calculated using the same

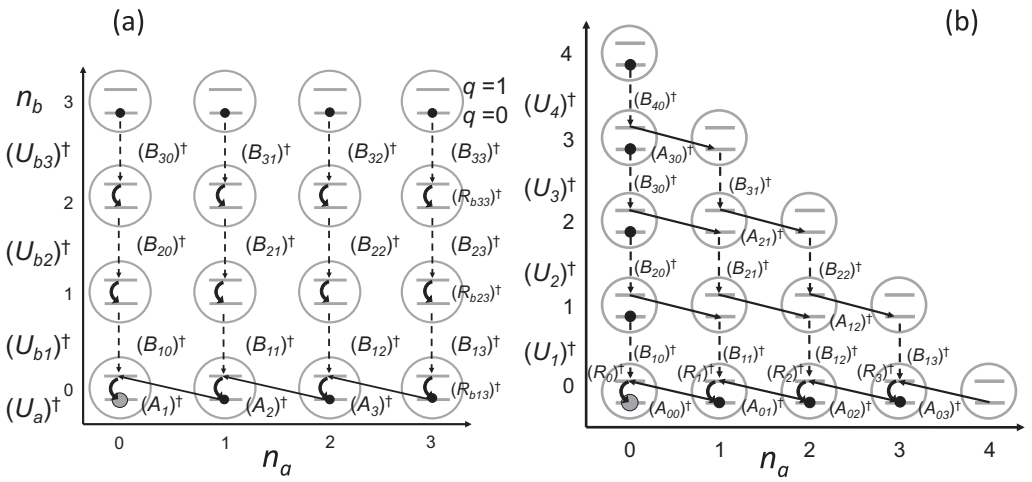

FIG. 3. Illustration of the Fock-state diagram for state synthesis. (a) Algorithm 1, the inverse sequence for the photon subtraction algorithm. (b) Algorithm 2, the inverse sequence for the photon swapping algorithm.

method. In more detail, $U_{b,j}^{\dagger}$ is a product of operations that subtract a photon from state $|0,k,j\rangle$ (transferring its amplitude to $|1,k-1,j\rangle$ and then to $|0,k-1,j\rangle$), first for $k=N_a\rightarrow 1$ (column by column), which is then repeated for $j=N_b\rightarrow 1$ (row by row). After all of the amplitudes have been transferred to the states $|0,k,0\rangle$, U_a removes these much as the original Law-Eberly algorithm. A graphical representation of this sequence is shown in Fig. 3(a).

To prevent amplitudes from returning to previously cleared states, it was proposed [21] to make the qubit rotations in $U_{b,j}$ number-state selective. This could be achieved by choosing a rotation for state $(n_a=k,n_b=j-1)$ only, but the main requirement is that previously removed states with $n_b=j$ and $n_a<k$ are unaffected. Note also that, for the number-state-selective interactions induced by coupling the resonator to a multilevel system, the column ordering may need to be reversed, as discussed in [36].

The actual steps involved in this algorithm are nearly identical to those in the Law-Eberly algorithm. The main challenge is to keep track of the various quantum states and the ordering of the operations. For completeness, we include an explicit treatment here, first breaking up the quantum evolution into two stages (for the B and A swaps, respectively). For the first stage, we define

$$\begin{aligned}|\psi_{j,k+1/2}\rangle &= B^{\dagger}(\theta_{jk})Z^{\dagger}(\alpha_{jk})|\psi_{j,k+1}\rangle,\\ |\psi_{j,k}\rangle &= R^{\dagger}_{n_a=k}(\gamma_{jk})Z^{\dagger}(\beta_{jk})|\psi_{j,k+1/2}\rangle,\end{aligned}\tag{53}$$

where k is the "fast" index (ranging from $N_a\rightarrow 0$) and j is the "slow" index (ranging from $N_b\rightarrow 1$). These states have the boundary conditions $|\psi_{j,N_a+1}\rangle=|\psi_{j+1,0}\rangle$ and $|\psi_{N_b,N_a+1}\rangle=|\psi_{\text{target}}\rangle$. Following a procedure similar to the previous section, we find

$$\begin{aligned}\alpha_{jk} &= \arg\left(\frac{\langle 1,k,j-1|\psi_{j,k+1}\rangle}{i\langle 0,k,j|\psi_{j,k+1}\rangle}\right),\\ \theta_{jk} &= \frac{1}{\sqrt{j}}\arctan\left(\left|\frac{\langle 0,k,j|\psi_{j,k+1}\rangle}{\langle 1,k,j-1|\psi_{j,k+1}\rangle}\right|\right),\\ \beta_{jk} &= \arg\left(\frac{i\langle 1,k,j-1|\psi_{j,k+1/2}\rangle}{\langle 0,k,j-1|\psi_{j,k+1/2}\rangle}\right),\\ \gamma_{jk} &= 2\arctan\left(\left|\frac{\langle 1,k,j-1|\psi_{j,k+1/2}\rangle}{\langle 0,k,j-1|\psi_{j,k+1/2}\rangle}\right|\right).\end{aligned}\tag{54}$$

These equations can be solved for $k=N_a\rightarrow 0$, $j=N_b\rightarrow 1$, until we reach the second stage.

For stage two, we define

$$\begin{aligned}|\psi_{j+1/2}\rangle &= A^{\dagger}(\theta_j)Z^{\dagger}(\alpha_j)|\psi_{j+1}\rangle,\\ |\psi_j\rangle &= R^{\dagger}(\gamma_j)Z^{\dagger}(\beta_j)|\psi_{j+1/2}\rangle,\end{aligned}\tag{55}$$

with j ranging from $N_a\rightarrow 1$ and $|\psi_{N_a+1}\rangle=|\psi_{1,1}\rangle$ (the final state from stage 1). The remaining parameters are then found by

$$\begin{aligned}\alpha_j &= \arg\left(\frac{\langle 1,j-1,0|\psi_{j+1}\rangle}{i\langle 0,j,0|\psi_{j+1}\rangle}\right),\\ \theta_j &= \frac{1}{\sqrt{j}}\arctan\left(\left|\frac{\langle 0,j,0|\psi_{j+1}\rangle}{\langle 1,j-1,0|\psi_{j+1}\rangle}\right|\right),\\ \beta_j &= \arg\left(\frac{i\langle 1,j-1,0|\psi_{j+1/2}\rangle}{\langle 0,j-1,0|\psi_{j+1/2}\rangle}\right),\\ \gamma_j &= 2\arctan\left(\left|\frac{\langle 1,j-1,0|\psi_{j+1/2}\rangle}{\langle 0,j-1,0|\psi_{j+1/2}\rangle}\right|\right).\end{aligned}\tag{56}$$

The total number of operations amounts to $N_a+N_b+N_aN_b$ swaps, $N_a+N_a+N_aN_b$ rotations, and $2(N_a+N_b+N_aN_b)$ phase shifts. Assuming we can turn the various Hamiltonians on and off with rates $\pm\Delta\omega$, g, and Ω (for the phase, swap, and rotation operators, respectively), the total time for this sequence is

$$\begin{aligned}T = &\frac{1}{\Delta\omega}\left(\sum_j(|\alpha_j|+|\beta_j|)+\sum_{jk}(|\alpha_{jk}|+|\beta_{jk}|)\right)\\ &+\frac{1}{\Omega}\left(\sum_j\gamma_j+\sum_{jk}\gamma_{jk}\right)+\frac{1}{g}\left(\sum_j\theta_j+\sum_{jk}\theta_{jk}\right).\end{aligned}\tag{57}$$

The averaged total angles are shown in Fig. 4. These were again formed by generating 100 random target states of the form Eq. (44) with $N_a=N_b=N_{\max}$ and summing and averaging the angles produced by Eqs. (54) and (56). Also shown are the approximations,

$$\begin{aligned}\sum_n\langle|\alpha_n|+|\beta_n|\rangle &\approx \pi\left(N_{\max}^2+\frac{3}{2}N_{\max}-\frac{1}{2}\right),\\ \sum_n\langle\gamma_n\rangle &\approx 2.8N_{\max}^2+4.6N_{\max}-2.7,\\ \sum_n\langle\theta_n\rangle &\approx 2.9N_{\max}-0.7,\end{aligned}\tag{58}$$

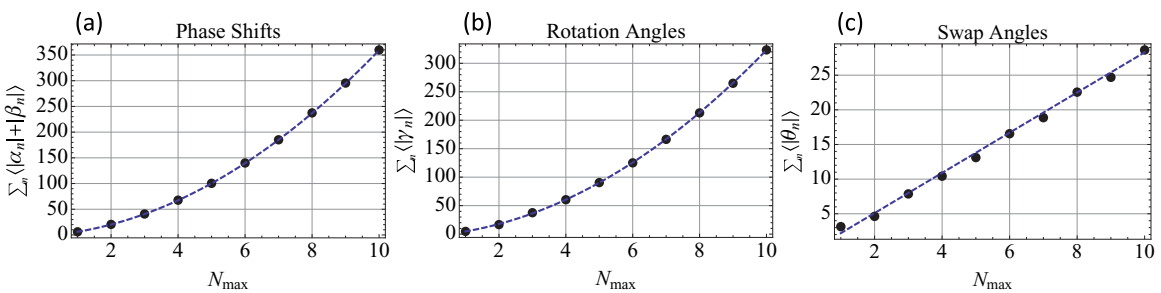

FIG. 4. Averaged total angles for the state synthesis sequence using the photon subtraction algorithm.

where the sums are over all of the indices (j,k) and j of stages one and two, respectively. The quadratic growth of the phase shifts and rotations match the total number of operations, while the linear growth of the swap angles is reduced by a square-root, similar to the Law-Eberly results above. We observe that the total time required to produce an arbitrary target state again scales with effective Hilbert-space dimension.

B. Algorithm 2: Photon swapping

An important fact regarding state synthesis is that the solution need not be unique. There are an infinite number of solutions, and finding the optimal solution, under constraints on time, energy, or complexity, is a hard problem [56,74]. For the algorithm just presented, we observe that each qubit rotation can add or remove one quantum of energy, which occurs $N_{\max}^2$ times. The desired state, however, has a maximum energy of $2N_{\max}$, corresponding to the resonator state $|N_{\max}\rangle \otimes |N_{\max}\rangle$. Thus, we might expect an optimal solution would use a smaller number of qubit rotations. We will provide such a solution in this section. For convenience, we will let the target state be a superposition of all states with quantum number $n_a + n_b \leqslant 2N_{\max}$:

$$|\psi\rangle = |0\rangle \otimes \sum_{n_a+n_b\leqslant 2N_{\max}} c_{n_a,n_b}|n_a\rangle \otimes |n_b\rangle. \tag{59}$$

The photon subtraction algorithm described above removes a quantum of energy for each and every possible state on the Fock-state diagram. However, one can just as easily move about the Fock-state diagram by swapping photons between the resonators, either directly or through the qubit [7]. Using the latter, we can swap photons along diagonal paths with a fixed number of quanta ($n_a + n_b + q = N_a + N_b \leqslant 2N_{\max}$). By first swapping all of the photons from resonator B to A, we can then remove a photon from mode A, after which we move to the next diagonal. By repeating the procedure, we need only use $2N_{\max}$ qubit rotations.

Specifically, our new algorithm is

$$U = \prod_{\ell=1}^{2N_{\max}} U_\ell, \tag{60}$$

where

$$U_\ell^\dagger = R_{n_a=\ell-1}^\dagger(\gamma_\ell)Z^\dagger(\phi_\ell)\prod_{m=\ell}^{1}[A^\dagger(\theta_{m-1,\ell-m}) \times Z^\dagger(\beta_{m-1,\ell-m})B^\dagger(\eta_{m,\ell-m})Z^\dagger(\alpha_{m,\ell-m})]. \tag{61}$$

The interpretation of each operation is analogous to Algorithm 1, however, the sequence of operations is significantly different. A graphical illustration of this photon swapping algorithm is presented in Fig. 3(b).

In this algorithm, as we move along the diagonal path with $n_a + n_b + q = \ell$, the operator $B^\dagger(\eta_{m,\ell-m})$ implements the transition $|0,\ell-m,m\rangle \to |1,\ell-m,m-1\rangle$, while for $m > 1$ $A^\dagger(\theta_{m-1,\ell-m})$ implements the transition $|1,\ell-m,m-1\rangle \to |0,\ell-m+1,m-1\rangle$. This sequence has the effect of repeatedly swapping quanta from mode B to mode A, until we reach $|1,\ell-1,0\rangle$. At this point, $\theta_{0,\ell-1}$ is chosen to complete the swapping transition $|0,\ell,0\rangle \to |1,\ell-1,0\rangle$, which is finally rotated to $|0,\ell-1,0\rangle$. This last step need only be selective on $n_a = \ell - 1$, and is so indicated in $U_\ell^\dagger$.

For completeness, we present the detailed steps of the algorithm. We again break each step in two by defining

$$\begin{aligned} |\psi_{\ell,m+1/2}\rangle &= B^\dagger(\eta_{m,\ell-m})Z^\dagger(\alpha_{m,\ell-m})|\psi_{\ell,m+1}\rangle, \\ |\psi_{\ell,m}\rangle &= A^\dagger(\theta_{m-1,\ell-m})Z^\dagger(\beta_{m-1,\ell-m})|\psi_{\ell,m_1/2}\rangle, \end{aligned} \tag{62}$$

where the various angles are calculated by the following equations:

$$\begin{aligned} \alpha_{m,\ell-m} &= \arg\left(\frac{\langle 1,\ell-m,m-1|\psi_{\ell,m+1}\rangle}{i\langle 0,\ell-m,m|\psi_{\ell,m+1}\rangle}\right), \\ \eta_{m,\ell-m} &= \frac{1}{\sqrt{m}}\arctan\left(\left|\frac{\langle 0,\ell-m,m|\psi_{\ell,m+1}\rangle}{\langle 1,\ell-m,m-1|\psi_{\ell,m+1}\rangle}\right|\right), \\ \beta_{m-1,\ell-m} &= \arg\left(\frac{i\langle 1,\ell-m,m-1|\psi_{\ell,m+1/2}\rangle}{\langle 0,\ell-m+1,m-1|\psi_{\ell,m+1/2}\rangle}\right), \\ \theta_{m-1,\ell-m} &= \frac{1}{\sqrt{\ell-m+1}} \\ &\quad\times\arctan\left(\left|\frac{\langle 1,\ell-m,m-1|\psi_{\ell,m+1/2}\rangle}{\langle 0,\ell-m+1,m-1|\psi_{\ell,m+1/2}\rangle}\right|\right). \end{aligned} \tag{63}$$

These can be solved from $m = \ell$ until $m = 1$, for which case we must modify our equations by

$$\begin{aligned} \beta_{0,\ell-1} &= \arg\left(\frac{\langle 1,\ell-1,0|\psi_{\ell,1+1/2}\rangle}{i\langle 0,\ell,0|\psi_{\ell,1+1/2}\rangle}\right), \\ \theta_{0,\ell-1} &= \frac{1}{\sqrt{\ell}}\arctan\left(\left|\frac{\langle 0,\ell,0|\psi_{\ell,1+1/2}\rangle}{\langle 1,\ell-1,0|\psi_{\ell,1+1/2}\rangle}\right|\right). \end{aligned} \tag{64}$$

This still leaves a final phase and amplitude rotation, the latter selective on $n_a = \ell - 1$, with parameters,

$$\begin{aligned} \phi_\ell &= \arg\left(\frac{i\langle 1,\ell-1,0|\psi_{\ell,1}\rangle}{\langle 0,\ell-1,0|\psi_{\ell,1}\rangle}\right), \\ \gamma_\ell &= 2\arctan\left(\left|\frac{\langle 1,\ell-1,0|\psi_{\ell,1}\rangle}{\langle 0,\ell-1,0|\psi_{\ell,1}\rangle}\right|\right). \end{aligned} \tag{65}$$

This sequence is then repeated for the next diagonal with $n_a + n_b + q = \ell - 1$, starting with $m = \ell - 1$ and $|\psi_{\ell-1,\ell}\rangle = |\psi_{\ell,1}\rangle$, and again for $\ell = 2N_{\max} \to 1$.

The expectation values for the sum of the angles, when averaged over many target states, are shown in Fig. 5, along with the approximate forms,

$$\begin{aligned} \sum_n \langle|\alpha_n| + |\beta_n| + |\phi_n|\rangle &\approx 6.4N_{\max}^2, \\ \sum_n \langle\gamma_n\rangle &\approx 6N_{\max} - 3, \\ \sum_n \langle\theta_n + \eta_n\rangle &\approx 1.65N_{\max}^2 + 4.2N_{\max} - 4.5. \end{aligned} \tag{66}$$

Here we see that the total rotation angles $\sum_n\langle\gamma_n\rangle$ is now *linear* with the maximum photon number, at the cost of an increased number of swaps (and phase rotations). However, this can represent a significant advantage, as the qubit rotations have (so far) been required to be number-state selective, and

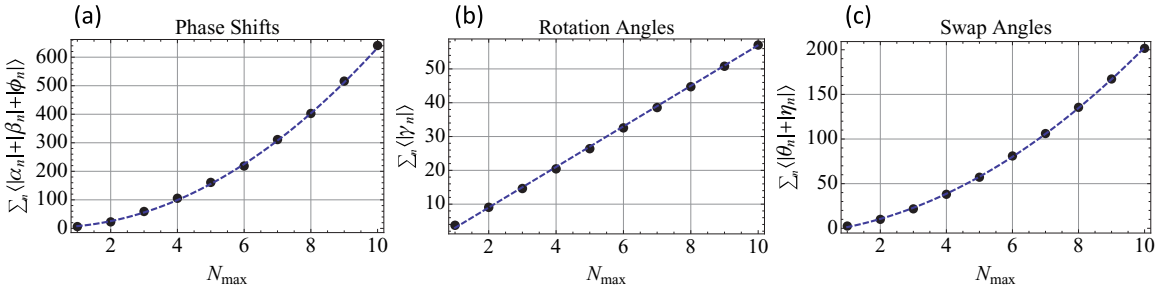

FIG. 5. Averaged total angles for the state synthesis sequence using the photon swapping algorithm.

thus limited in Rabi amplitude Ω [36]. By reducing the number of such rotations, the total time can be reduced. The overall scaling of the time, however, is again proportional to the effective Hilbert-space dimension.

V. SPECIAL TWO-RESONATOR STATES

The algorithms presented above are designed for the synthesis of an arbitrary state of two resonators. For many applications, the desired target state has a specific form. One such target state is the so-called NOON state:

$$|\psi_{\text{target}}\rangle = |0\rangle \otimes \frac{1}{\sqrt{2}}(|N,0\rangle + |0,N\rangle), \tag{67}$$

an entangled superposition of resonator states in which N photons are in mode A or mode B. This state can be considered a generalization of the Bell and GHZ states, and has potential applications in quantum metrology [75]. A second such target state is the maximally entangled state,

$$|\psi_{\text{target}}\rangle = \frac{1}{\sqrt{N}} \sum_{n=0}^{N} |N-n,n\rangle. \tag{68}$$

This state can be used for tests of higher-dimensional Bell inequalities [76] and superdense teleportation [77]. In this section we analyze how the photon subtraction and photon swapping algorithms perform for these two important entangled states. In fact, we find that the photon swapping algorithm can prepare any state of the form,

$$|\psi_{\text{target}}\rangle = |0\rangle \otimes \sum_{n=0}^{N} c_n |N-n,n\rangle, \tag{69}$$

without state-selective interactions.

A. NOON state synthesis

The NOON state has the special status of having entanglement equal to that of a singlet state. As such, it can be prepared without using the full algorithms described above. Indeed, the initial experiment to generate a "high" NOON state (with $N = 3$) was performed using a particular preparation method [22,38]. That method uses a pair of three-level systems to couple the resonators. This method has been simplified using a single three-level system [23] or four levels of a tunable flux-based device [24]. These methods start from a single superposition state of the auxiliary system that is then mapped onto the resonators, and require state-selective swapping interactions that are effectively turned on and off by tuning the auxiliary system.

While these methods do not require number-state-selective transitions, their use of state-selective swaps limits the coupling rate due to the anharmonicity of the system [11]. Nevertheless, these methods can be implemented faster than the original state-synthesis algorithm [21] (the photon subtraction method presented above). However, a comparison with the experimental method [22,38] showed that both were experimentally comparable as far as decoherence is concerned [36]. Here we consider the new photon swapping algorithm and show that no multilevel systems or state-selective interactions are required, allowing for faster operations and simplified experimental design.

This improved performance is due to the nature of the paths taken through the Fock-space diagram in this new algorithm. By following the photon swapping method, starting from a superposition of a given diagonal $n_a + n_b = N$, the first time through one can move all of the population down to $|0,N-1,0\rangle$. Thus, one need only use a Law-Eberly sequence along the path $n_b = 0$ to remove the photons from the system. The result is that *any* "diagonal" state of the form Eq. (69) can be synthesized by one sequence of photon swaps followed by a Law-Eberly sequence with no state-selective interactions. The specific set of parameters for NOON state synthesis with $N = 3$ are shown for the photon subtraction and swapping algorithms are shown in Tables I and II, respectively, and graphically represented in Fig. 6.

We now compare these two approaches for a general NOON state. Based on previous analysis [36], we find that the photon

TABLE I. NOON state synthesis by the photon subtraction algorithm.

Step	Parameters	Quantum state
R_1	$\gamma_1 = \pi/2$	$\|0,0,0\rangle - i\|1,0,0\rangle$
A_1	$\theta_1 = \pi$	$\|0,0,0\rangle - \|0,1,0\rangle$
R_2	$\gamma_2 = \pi$	$\|0,0,0\rangle + i\|1,1,0\rangle$
A_2	$\theta_2 = \pi/\sqrt{2}$	$\|0,0,0\rangle + \|0,2,0\rangle$
R_3	$\gamma_2 = \pi$	$\|0,0,0\rangle - i\|1,2,0\rangle$
A_3	$\theta_3 = \pi/\sqrt{3}$	$\|0,0,0\rangle - \|0,3,0\rangle$
R_4	$\gamma_2 = \pi$	$-i\|1,0,0\rangle - \|0,3,0\rangle$
B_1	$\eta_1 = \pi$	$-\|0,0,1\rangle - \|0,3,0\rangle$
R_5	$\gamma_2 = \pi$	$i\|1,0,1\rangle - \|0,3,0\rangle$
B_2	$\eta_2 = \pi/\sqrt{2}$	$\|0,0,2\rangle - \|0,3,0\rangle$
R_6	$\gamma_2 = \pi$	$-i\|1,0,2\rangle - \|0,3,0\rangle$
B_3	$\eta_3 = \pi/\sqrt{3}$	$-\|0,0,3\rangle - \|0,3,0\rangle$

TABLE II. NOON state synthesis by the photon swapping algorithm.

Step	Parameters	Quantum state
R_1	$\gamma_1 = \pi$	$-i\|1,0,0\rangle$
A_1	$\theta_1 = \pi/2$	$-\|0,1,0\rangle$
R_2	$\gamma_2 = \pi$	$+i\|1,1,0\rangle$
A_2	$\theta_2 = \pi/2\sqrt{2}$	$+\|0,2,0\rangle$
R_3	$\gamma_3 = \pi$	$-i\|1,2,0\rangle$
A_3	$\theta_3 = 0.2153$	$-0.3643\|0,3,0\rangle - i0.9313\|1,2,0\rangle$
B_1	$\eta_1 = 2.1999$	$-0.3643\|0,3,0\rangle + i0.548\|1,2,0\rangle - 0.753\|0,2,1\rangle$
A_4	$\theta_4 = 1.3589$	$+0.6454\|0,3,0\rangle - i0.1283\|1,2,0\rangle + 0.2589\|0,2,1\rangle + i0.7071\|1,1,1\rangle$
B_2	$\eta_2 = \pi/2\sqrt{2}$	$+0.6454\|0,3,0\rangle - i0.2889\|1,2,0\rangle + 0.7071\|0,1,2\rangle$
A_5	$\theta_5 = \pi/2$	$-0.7071\|0,3,0\rangle - i0.7071\|1,0,2\rangle$
B_3	$\eta_3 = \pi/2\sqrt{3}$	$-0.7071\|0,3,0\rangle - 0.7071\|0,3,0\rangle$

subtraction method requires N A swaps, N B swaps, and $2N$ rotations. No phase shifts are required, and the parameters scale as

$$\begin{aligned}\left(\sum_n \gamma_n\right)_{\text{subtraction}} &\approx \pi\left(2N_{\max} - \frac{1}{2}\right),\\ \left(\sum_n [\theta_n + \eta_n]\right)_{\text{subtraction}} &\approx 6\sqrt{N_{\max}} - 3.3.\end{aligned} \tag{70}$$

As in the general photon subtraction algorithm, many of these rotations must be number-state selective.

The photon swapping algorithm requires $2N-1$ A swaps, N B swaps, and N rotations. There are also a few phase shifts required, but they do not scale appreciably with N. By looking at the numerical performance for the NOON state (not shown), we find

$$\begin{aligned}\left(\sum_n \gamma_n\right)_{\text{swapping}} &\approx \pi N_{\max},\\ \left(\sum_n [\theta_n + \eta_n]\right)_{\text{swapping}} &\approx 9.9\sqrt{N_{\max}} - 9.2.\end{aligned} \tag{71}$$

As described above, these rotations need not be number-state selective.

Comparing these two algorithms for the NOON state, we see that we have traded rotations for swaps, with the photon swapping algorithm achieving the minimal number of rotations. Even better, the photon swapping method does not require those rotations to be state selective. This advantage is particularly nice as the actual dispersive shifts for a multilevel system coupled to a resonator can be quite complicated [9,11,78] and the extension to multiple resonators is an outstanding experimental challenge [43]. There is also an advantage over the special-purpose algorithms in terms of reduced complexity of hardware and controls [22–24]. Thus, the method presented here has both theoretical and experimental advantages, with the potential for fast performance and optimal scaling.

B. Maximally entangled states

While most research has studied NOON state synthesis, the maximally entangled states of Eq. (68) are of potentially greater value. As discussed above, the photon swapping algorithm can produce a superposition along the diagonals of the Fock state diagram with only N rotations. For the

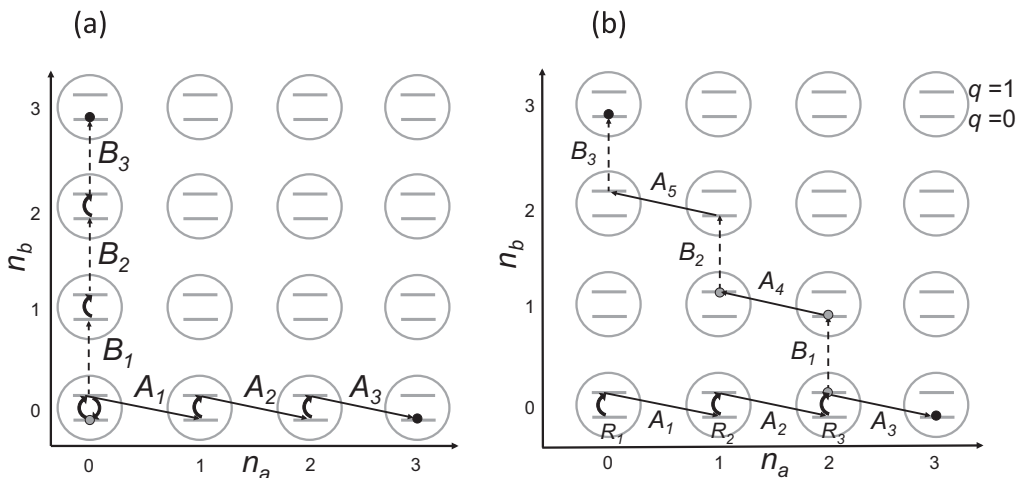

FIG. 6. NOON state synthesis (with $N = 3$) using (a) the photon subtraction method, and (b) the photon swapping method. Both prepare the NOON state with a linear number of steps, but the latter uses no state-selective interactions.

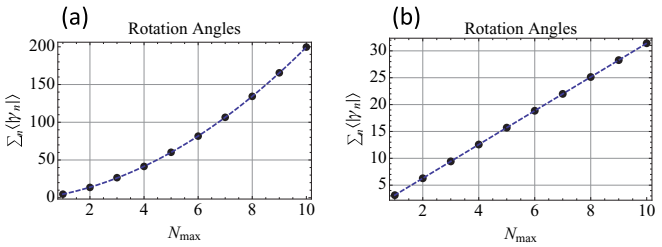

FIG. 7. Total rotation angles for the state synthesis of the maximally entangled state using (a) the photon subtraction algorithm, and (b) the photon swapping algorithm.

maximally entangled states we compare the rotations required by two state-synthesis algorithms in Fig. 7.

We find that the photon subtraction algorithm requires a quadratic number of rotations, with the total of the rotation angles scaling as

$$\left(\sum_n \gamma_n\right)_{\text{subtraction}} \approx 1.56N_{\max}^2 + 4.49N_{\max} - 1.33. \quad (72)$$

Here many of the rotations must be number-state selective. However, the photon swapping algorithm, as argued above, requires only N rotations, with the total of the rotation angles scaling as

$$\left(\sum_n \gamma_n\right)_{\text{swapping}} \approx \pi N_{\max}. \quad (73)$$

Here *none* of the rotations need be number-state selective. We thus see that the photon swapping algorithm achieves the same advantages found for NOON state synthesis, with both a reduced number of rotations and the elimination of their number-state-selective character.

VI. CONCLUSION

In this paper, we have studied state synthesis algorithms for superconducting resonators. Starting from a qudit and the classic Law-Eberly algorithm, we have explored how solving for the inverse evolution allows one to determine the operations needed to synthesize an arbitrary state. We have further shown how these step-by-step procedures have a complexity that typically grows linearly with the effective Hilbert-space dimension. These schemes have been extended to two different state synthesis algorithms for a qubit coupled to two resonators. The first uses photon subtraction to ensure that the inverse evolution leads to the ground state, whereas the second uses photon swapping before any photons are removed from the system. When taken in reverse, these algorithms allow one to synthesize an arbitrary entangled state of two resonators. Finally, when applied to typical superconducting circuit experiments, we expect that the photon swapping method will have improved performance due to a reduced number of state-selective interactions.

While we have found an improved algorithm, we do not claim to have found an optimal algorithm. Indeed, we believe that numerical optimizations using the same basic Hamiltonians can lead to improved methods for state synthesis. However, we do hold that the two algorithms compared here are the most natural analytical approaches to state synthesis. At the same time, the differences between the two algorithms suggest that different types of optimizations may be possible. The photon subtraction algorithm minimizes the number of A swaps performed on the system, but at the cost of a quadratic number of B swaps and state-selective qubit rotations. By contrast, the photon swapping algorithm minimizes the number of rotations, at the cost of an increased number of A swaps and slightly increased overall complexity. Nevertheless, for states such as the NOON and maximally entangled states, the photon swapping method appears to have overall better performance, in that no state-selective rotations are needed at all.

Finally, the *linear* scaling of the NOON state sequences are nearly ideal, in that the energy of the final state and the number of qubit rotations used (to put energy into the system) are both linear in the state number $N_{\max}$ [11]. We further observe that one can achieve a reduction in time complexity by a factor of two by driving multiple transitions simultaneously [26], but the linear scaling remains. However, recent work has found, using numerical optimization, that sublinear scaling is possible for Fock state preparation by starting the cavity in a large-amplitude coherent state and using repeated number-state-dependent qubit transitions and displacements of the resonator [28]. Extending such a scheme to NOON state synthesis in two cavities using two qubits is straightforward [26]; whether a single qubit suffices is an interesting question.

In conclusion, we have improved the theoretical understanding and performance of entangled-state synthesis algorithms for superconducting resonators. We hope that the results presented here, on a fundamental quantum control problem, may provide useful benchmarks for future explorations of control of superconducting or other resonator-based systems.

ACKNOWLEDGMENTS

This work was supported by the NSF under Projects No. PHY-1005571 and No. PHY-1212413. We gratefully acknowledge discussions with Q. Zhang and R. W. Simmonds.

APPENDIX: DRIVEN TWO-MODE JAYNES-CUMMINGS HAMILTONIAN

In this appendix we derive the effective Hamiltonians used in Sec. IV in the text, starting from the driven two-mode Jaynes-Cummings Hamiltonian,

$$\mathcal{H}/\hbar = \omega_a a^\dagger a + \omega_b b^\dagger b + \omega_q(t)\sigma^\dagger\sigma + F(t)\sigma_x + g_a(t)(\sigma^\dagger a + \sigma a^\dagger) + g_b(t)(\sigma^\dagger b + \sigma b^\dagger). \quad (A1)$$

This Hamiltonian models two resonators with different frequencies ($\omega_a \neq \omega_b$) and coupled by a qubit. Ideally, the qubit has a tunable frequency $\omega_q(t)$, is controllably coupled to each resonator [with couplings $g_a(t)$ and $g_b(t)$], and is driven by an external control field $F(t)$. While such a system has not yet been realized, the effective Hamiltonians used in the text can be realized using experimentally demonstrated interactions: Systems with fixed couplings (and a tunable qubit frequency) have been realized in [7] and [45]; systems

with controllable couplings have been realized in a number of different ways [46–52].

We will consider both fixed and controllable couplings in this appendix, and describe three primary modes of operation. The first mode involves operations in the dispersively coupled regime (when $|\omega_q - \omega_a|, |\omega_q - \omega_b| \gg g_a, g_b$), with fixed couplings. The second mode involves operations in the resonant regime (when $\omega_q = \omega_a$ or $\omega_q = \omega_b$), again with fixed couplings. These two modes can be accessed by using a qubit with a dynamically tunable frequency $\omega_q(t)$ [42,43]. The third mode involves time-dependent parametric couplings [48,51] that can be used to generate operations with a fixed frequency qubit (with $\omega_q \neq \omega_a, \omega_b$).

1. Dispersive regime

In the dispersive regime, we analyze the dynamics using a canonical transformation [79],

$$\mathcal{H}' = e^{K} \mathcal{H} e^{-K}, \tag{A2}$$

with

$$K = \frac{g_a}{\Delta_a}(a^\dagger \sigma - a \sigma^\dagger) + \frac{g_b}{\Delta_b}(b^\dagger \sigma - b \sigma^\dagger), \tag{A3}$$

where g_a and g_b are held constant and we have defined $\Delta_a = \omega_a - \omega_0$ and $\Delta_b = \omega_b - \omega_0$, with ω_0 a constant idling point of the qubit frequency. By expanding the exponentials to second order in the couplings, one obtains (with $F = 0$ and $\omega_q = \omega_0$)

$$\begin{aligned} \mathcal{H}'/\hbar \approx & \left(\omega_a + \frac{g_a^2}{\Delta_a}\right) a^\dagger a + \left(\omega_b + \frac{g_b^2}{\Delta_b}\right) b^\dagger b \\ & + \frac{g_a g_b}{2}\left(\frac{1}{\Delta_a} + \frac{1}{\Delta_b}\right)(a^\dagger b + a b^\dagger)\sigma_z \\ & + \left[\omega_0 - \frac{g_a^2}{\Delta_a}(2n_a + 1) - \frac{g_b^2}{\Delta_b}(2n_b + 1)\right]\sigma^\dagger \sigma, \end{aligned} \tag{A4}$$

where $n_a = a^\dagger a$ and $n_b = b^\dagger b$.

This transformation has produced small shifts of the resonator frequencies, a small coupling term, and a number-state-dependent shift of the qubit frequency (the ac Stark shift). By additional transformations, we can simplify this Hamiltonian to that used in the text. Specifically, we can remove the first two terms in Eq. (A4) by a rotating frame transformation for the resonators and the third by a rotating wave approximation (using the fact that $|\omega_a - \omega_b| > g_a, g_b$ in the dispersive regime). By reintroducing the detuning and the coupling field, we thus obtain the effective Hamiltonian,

$$\begin{aligned} \mathcal{H}''/\hbar \approx & \, \Delta\omega(t)\sigma^\dagger \sigma + \sum_{n_a, n_b} \omega_{n_a, n_b} \Pi_{n_a, n_b} \sigma^\dagger \sigma \\ & + F(t) \sum_{n_a, n_b} \Pi_{n_a, n_b} \sigma_x, \end{aligned} \tag{A5}$$

where we have used the projection operators,

$$\Pi_{n_a, n_b} = |n_a, n_b\rangle\langle n_a, n_b|, \tag{A6}$$

and defined the time-dependent detuning $\Delta\omega(t) = \omega_q(t) - \omega_0$ and the number-state-dependent qubit transition frequencies,

$$\omega_{n_a, n_b} = \left[\omega_0 - \frac{g_a^2}{\Delta_a}(2n_a + 1) - \frac{g_b^2}{\Delta_b}(2n_b + 1)\right]. \tag{A7}$$

We proceed to consider Eq. (A5) when the driving field drives all of the number-state-dependent transitions in parallel:

$$F(t) = \sum_{n_a, n_b} \Omega_{n_a, n_b} \cos\left(\omega_{n_a, n_b} t\right), \tag{A8}$$

and perform yet another rotating frame transformation and rotating wave approximation. This can be done by using the transformation,

$$\mathcal{H}_{\text{eff}} = U_0^\dagger \mathcal{H}'' U_0 - i\hbar U_0^\dagger dU_0/dt, \tag{A9}$$

with

$$U_0 = \exp\left(-it \sum_{n_a, n_b} \omega_{n_a, n_b} \Pi_{n_a, n_b} \sigma^\dagger \sigma\right), \tag{A10}$$

and selecting the time-independent terms, which yields

$$\mathcal{H}_{\text{eff}}/\hbar \approx \Delta\omega \sigma^\dagger \sigma + \frac{1}{2} \sum_{n_a, n_b} \Omega_{n_a, n_b} \Pi_{n_a, n_b} \sigma_x. \tag{A11}$$

This expression agrees with the effective Hamiltonian (with $g_a, g_b \to 0$) of Eq. (45) in the text. Number-state-dependent transitions can be driven provided the Rabi frequencies Ω_{n_a, n_b} are small compared to the frequency differences $|\omega_{n_a+1, n_b} - \omega_{n_a, n_b}| = 2g_a^2/\Delta_a$ and $|\omega_{n_a, n_b+1} - \omega_{n_a, n_b}| = 2g_b^2/\Delta_b$; this ensures that the rotating wave approximation remains valid. Small changes of $\Delta\omega$ about zero will cause the qubit state to develop a phase with respect to the driving field (which is what is observed in tomography [20]). We note that these results can be extended to coupling of resonators via a multilevel system, albeit with modified number-state-dependent qubit transition frequencies [9,11,78]; some of the implications of these modified results have been discussed elsewhere [36]. The conclusions of this paper are largely independent of these modifications.

2. Resonant regime

In the resonant regime, we have $\omega_q = \omega_a$ or $\omega_q = \omega_b$. In these cases, a rotating frame transformation (and rotating wave approximation) yield the qubit-resonator swapping interactions,

$$\mathcal{H}_{\text{eff}}/\hbar = g_a(\sigma^\dagger a + \sigma a^\dagger), \tag{A12}$$

and

$$\mathcal{H}_{\text{eff}}/\hbar = g_b(\sigma^\dagger b + \sigma b^\dagger), \tag{A13}$$

respectively. These agree with the effective Hamiltonian (with $\Delta\omega, \Omega_{n_a, n_b} \to 0$) of Eq. (45) in the text. While there are residual phase shifts incurred by tuning the qubit frequency between these two frequencies, these phases can be adjusted (relative to the fixed condition $\Delta\omega = 0$ discussed above) during the time-dependent pulse [40,41].

3. Parametric coupling

The previous mode of operation required a qubit with a tunable frequency. A fixed frequency qubit will require an alternative mode of operation, which is possible using parametric coupling. Such methods have been experimentally demonstrated and used to couple a qubit and lumped-element resonator [48], two planar resonators [51], and two

three-dimensional cavities [52]. These experiments all use a parametric coupling of the form,

$$g(t) = g_0 + g_1 \cos(\omega t). \tag{A14}$$

This type of coupling can achieve the two modes of operation described above in the following way. First, one can operate the coupler with $g_0 \neq 0$ and $g_1 = 0$ to effect the number-state-dependent transitions in the dispersive regime. Second, one can operate the coupler with $g_0 = 0$, $g_1 \neq 0$, and ω tuned to the difference in frequencies $\omega_a - \omega_q$ or $\omega_b - \omega_q$ to effect the qubit-resonator swapping interactions in the resonant regime. Thus, all of the operations designed for systems with tunable frequency qubits and fixed couplings can be realized for fixed frequency qubits and tunable couplings.

[1] M. H. Devoret, D. Esteve, J. M. Martinis, and C. Urbina, Phys. Scr. T **25**, 118 (1989).

[2] I. Chiorescu, P. Bertet, K. Semba, Y. Nakamura, C. J. P. M. Harmans, and J. E. Mooij, Nature (London) **431**, 159 (2004).

[3] A. Wallraff, D. I. Schuster, A. Blais, L. Frunzio, R.-S. Huang, J. Majer, S. Kumar, S. M. Girvin, and R. J. Schoelkopf, Nature (London) **431**, 162 (2004).

[4] H. Xu, F. W. Strauch, S. K. Dutta, P. R. Johnson, R. C. Ramos, A. J. Berkley, H. Paik, J. R. Anderson, A. J. Dragt, C. J. Lobb, and F. C. Wellstood, Phys. Rev. Lett. **94**, 027003 (2005).

[5] R. J. Schoelkopf and S. M. Girvin, Nature (London) **451**, 664 (2008).

[6] M. Mariantoni, H. Wang, T. Yamamoto, M. Neeley, R. Bialczak, Y. Chen, M. Lenander, E. Lucero, A. D. O'Connell, D. Sank *et al.*, Science **334**, 61 (2011).

[7] M. Mariantoni, H. Wang, R. Bialczak, M. Lenander, E. Lucero, M. Neeley, A. D. O'Connell, D. Sank, M. Weides, J. Wenner *et al.*, Nat. Phys. **7**, 287 (2011).

[8] H. Paik, D. I. Schuster, L. S. Bishop, G. Kirchmair, G. Catelani, A. P. Sears, B. R. Johnson, M. J. Reagor, L. Frunzio, L. I. Glazman *et al.*, Phys. Rev. Lett. **107**, 240501 (2011).

[9] M. Boissonneault, J. M. Gambetta, and A. Blais, Phys. Rev. Lett. **105**, 100504 (2010).

[10] L. S. Bishop, E. Ginossar, and S. M. Girvin, Phys. Rev. Lett. **105**, 100505 (2010).

[11] F. W. Strauch, Phys. Rev. A **84**, 052313 (2011).

[12] S. E. Nigg and S. M. Girvin, Phys. Rev. Lett. **110**, 243604 (2013).

[13] Z. Leghtas, G. Kirchmair, B. Vlastakis, R. J. Schoelkopf, M. H. Devoret, and M. Mirrahimi, Phys. Rev. Lett. **111**, 120501 (2013).

[14] S. Haroche and J.-M. Raimond, *Exploring the Quantum* (Oxford University Press, Oxford, 2006).

[15] E. Brion, K. Mølmer, and M. Saffman, Phys. Rev. Lett. **99**, 260501 (2007).

[16] J. Refsgaard and K. Mølmer, Phys. Rev. A **86**, 022302 (2012).

[17] A. D. O'Connell, M. Hofheinz, M. Ansmann, R. C. Bialczak, M. Lenander, E. Lucero, M. Neeley, D. Sank, H. Wang, M. Weides *et al.*, Nature (London) **464**, 697 (2010).

[18] F. Lecocq, J. D. Teufel, J. Aumentado, and R. W. Simmonds, Nat. Phys. **11**, 635 (2015).

[19] M. Hofheinz, E. M. Weig, M. Ansmann, R. C. Bialczak, E. Lucero, M. Neeley, A. D. O'Connell, H. Wang, J. M. Martinis, and A. N. Cleland, Nature (London) **454**, 310 (2008).

[20] M. Hofheinz, H. Wang, M. Ansmann, R. C. Bialczak, E. Lucero, M. Neeley, A. D. O'Connell, D. Sank, J. Wenner, J. M. Martinis *et al.*, Nature (London) **459**, 546 (2009).

[21] F. W. Strauch, K. Jacobs, and R. W. Simmonds, Phys. Rev. Lett. **105**, 050501 (2010).

[22] S. T. Merkel and F. K. Wilhelm, New J. Phys. **12**, 093036 (2010).

[23] Q.-P. Su, C.-P. Yang, and S.-B. Zheng, Sci. Rep. **4**, 3898 (2014).

[24] S.-J. Xiong, T. Lie, J.-M. Liu, and C.-P. Yang, Opt. Lett. **40**, 2221 (2015).

[25] M. F. Santos, Phys. Rev. Lett. **95**, 010504 (2005).

[26] F. W. Strauch, Phys. Rev. Lett. **109**, 210501 (2012).

[27] B. Mischuck and K. Mølmer, Phys. Rev. A **87**, 022341 (2013).

[28] S. Krastanov, V. V. Albert, C. Shen, C.-L. Zou, R. W. Heeres, B. Vlastakis, R. Schoelkopf, and L. Jiang, Phys. Rev. A **92**, 040303(R) (2015).

[29] D. Gottesman, Chaos Solitons Fractals **10**, 1749 (1999).

[30] Z. Leghtas, G. Kirchmair, B. Vlastakis, M. H. Devoret, R. J. Schoelkopf, and M. Mirrahimi, Phys. Rev. A **87**, 042315 (2013).

[31] F. Xue, Y. X. Liu, C. P. Sun, and F. Nori, Phys. Rev. B **76**, 064305 (2007).

[32] M. Mariantoni, F. Deppe, A. Marx, R. Gross, F. K. Wilhelm, and E. Solano, Phys. Rev. B **78**, 104508 (2008).

[33] F. L. Semiao, K. Furuya, and G. J. Milburn, Phys. Rev. A **79**, 063811 (2009).

[34] S. Kumar and D. P. DiVincenzo, Phys. Rev. B **82**, 014512 (2010).

[35] A. V. Sharypov, X. Deng, and L. Tian, Phys. Rev. B **86**, 014516 (2012).

[36] F. W. Strauch, D. Onyango, K. Jacobs, and R. W. Simmonds, Phys. Rev. A **85**, 022335 (2012).

[37] C. K. Law and J. H. Eberly, Phys. Rev. Lett. **76**, 1055 (1996).

[38] H. Wang, M. Mariantoni, R. C. Bialczak, M. Lenander, E. Lucero, M. Neeley, A. D. O'Connell, D. Sank, M. Weides, J. Wenner *et al.*, Phys. Rev. Lett. **106**, 060401 (2011).

[39] D. I. Schuster, A. A. Houck, J. A. Schreier, A. Wallraff, J. M. Gambetta, A. Blais, L. Frunzio, J. Majer, B. Johnson, M. H. Devoret *et al.*, Nature (London) **445**, 515 (2007).

[40] L. DiCarlo, J. M. Chow, J. M. Gambetta, L. S. Bishop, B. R. Johnson, D. I. Schuster, J. Majer, A. Blais, L. Frunzio, S. M. Girvin *et al.*, Nature (London) **460**, 240 (2009).

[41] L. DiCarlo, M. D. Reed, L. Sun, B. R. Johnson, J. M. Chow, J. M. Gambetta, L. Frunzio, S. M. Girvin, M. H. Devoret, and R. J. Schoelkopf, Nature (London) **467**, 574 (2010).

[42] B. R. Johnson, M. D. Reed, A. A. Houck, D. I. Schuster, L. S. Bishop, E. Ginossar, J. M. Gambetta, L. DiCarlo, L. Frunzio, S. M. Girvin, and R. J. Schoelkopf, Nat. Phys. **6**, 663 (2010).

[43] B. R. Johnson, Ph.D. thesis, Yale University, 2011.

[44] I. M. Pop, K. Geerlings, G. Catelani, R. J. Schoelkopf, L. I. Glazman, and M. H. Devoret, Nature (London) **508**, 369 (2014).

[45] M. D. Reed, Ph.D. thesis, Yale University, 2013.

[46] M. S. Allman, F. Altomare, J. D. Whittaker, K. Cicak, D. Li, A. Sirois, J. Strong, J. D. Teufel, and R. W. Simmonds, Phys. Rev. Lett. **104**, 177004 (2010).
[47] R. C. Bialczak, M. Ansmann, M. Hofheinz, M. Lenander, E. Lucero, M. Neeley, A. O'Connell, D. Sank, H. Wang, M. Weides *et al.*, Phys. Rev. Lett. **106**, 060501 (2011).
[48] M. S. Allman, J. D. Whittaker, M. Castellanos-Beltran, K. Cicak, F. da Silva, M. P. DeFeo, F. Lecocq, A. Sirois, J. D. Teufel, J. Aumentado *et al.*, Phys. Rev. Lett. **112**, 123601 (2014).
[49] S. Zeytinoglu, M. Pechal, S. Berger, A. A. Abdumalikov, Jr., A. Wallraff, and S. Filipp, Phys. Rev. A **91**, 043846 (2015).
[50] Y. Chen, C. Neill, P. Roushan, N. Leung, M. Fang, R. Barends, J. Kelly, B. Campbell, Z. Chen, B. Chiaro *et al.*, Phys. Rev. Lett. **113**, 220502 (2014).
[51] E. Zakka-Bajjani, F. Nguyen, M. Lee, L. R. Vale, R. W. Simmonds, and J. Aumentado, Nat. Phys. **7**, 599 (2011).
[52] A. J. Sirois, M. A. Castellanos-Beltran, M. P. DeFeo, L. Ranzani, F. Lecocq, R. W. Simmonds, J. D. Teufel, and J. Aumentado, Appl. Phys. Lett. **106**, 172603 (2015).
[53] A. Wallraff, D. I. Schuster, A. Blais, J. M. Gambetta, J. Schreier, L. Frunzio, M. H. Devoret, S. M. Girvin, and R. J. Schoelkopf, Phys. Rev. Lett. **99**, 050501 (2007).
[54] P. J. Leek, S. Filipp, P. Maurer, M. Baur, R. Bianchetti, J. M. Fink, M. Goppl, L. Steffen, and A. Wallraff, Phys. Rev. B **79**, 180511(R) (2009).
[55] J. D. Strand, M. Ware, F. Beaudoin, T. A. Ohki, B. R. Johnson, A. Blais, and B. L. T. Plourde, Phys. Rev. B **87**, 220505 (2013).
[56] K. W. Moore and H. Rabitz, Phys. Rev. A **84**, 012109 (2011).
[57] J. Kerckhoff, R. W. Andrews, H. S. Ku, W. F. Kindel, K. Cicak, R. W. Simmonds, and K. W. Lehnert, Phys. Rev. X **3**, 021013 (2013).
[58] L. C. G. Govia, E. J. Pritchett, and F. Wilhelm, arXiv:1210.4042.
[59] A. Muthukrishnan and C. R. Stroud, Phys. Rev. A **62**, 052309 (2000).
[60] G. K. Brennen, D. P. O'Leary, and S. S. Bullock, Phys. Rev. A **71**, 052318 (2005).
[61] S. S. Bullock, D. P. O'Leary, and G. K. Brennen, Phys. Rev. Lett. **94**, 230502 (2005).
[62] D. P. O'Leary, G. K. Brennen, and S. S. Bullock, Phys. Rev. A **74**, 032334 (2006).
[63] T. C. Ralph, K. J. Resch, and A. Gilchrist, Phys. Rev. A **75**, 022313 (2007).
[64] B. P. Lanyon, M. Barbieri, M. P. Almeida, T. Jennewein, T. C. Ralph, K. J. resch, G. J. Pryde, J. L. O'Brien, A. Gilchrist, and A. G. White, Nat. Phys. **5**, 134 (2009).
[65] S. D. Bartlett, H. de Guise, and B. C. Sanders, Phys. Rev. A **65**, 052316 (2002).
[66] M. Neeley, M. Ansmann, R. C. Bialczak, M. Hofheinz, E. Lucero, A. D. O'Connell, D. Sank, H. Wang, J. Wenner, A. N. Cleland *et al.*, Science **325**, 722 (2009).
[67] A. Ben-Kish, B. DeMarco, V. Meyer, M. Rowe, J. Britton, W. M. Itano, B. M. Jelenković, C. Langer, D. Leibfried, T. Rosenband *et al.*, Phys. Rev. Lett. **90**, 037902 (2003).
[68] E. T. Jaynes and F. W. Cummings, Proc. IEEE **51**, 89 (1963).
[69] S. A. Gardiner, J. I. Cirac, and P. Zoller, Phys. Rev. A **55**, 1683 (1997).
[70] J. Steinbach, J. Twamley, and P. L. Knight, Phys. Rev. A **56**, 4815 (1997).
[71] G. Drobný, B. Hladký, and V. Bužek, Phys. Rev. A **58**, 2481 (1998).
[72] B. Kneer and C. K. Law, Phys. Rev. A **57**, 2096 (1998).
[73] S.-B. Zheng, Phys. Rev. A **63**, 015801 (2000).
[74] K. W. Moore, R. Chakrabarti, G. Riviello, and H. Rabitz, Phys. Rev. A **83**, 012326 (2011).
[75] J. P. Dowling, Contemp. Phys. **49**, 125 (2008).
[76] A. C. Dada, J. Leach, G. S. Buller, M. J. Padgett, and E. Andersson, Nat. Phys. **7**, 677 (2011).
[77] T. M. Graham, H. J. Berstein, T.-C. Wei, M. Junge, and P. G. Kwiat, Nat. Commun. **6**, 7185 (2015).
[78] J. Koch, T. M. Yu, J. Gambetta, A. A. Houck, D. I. Schuster, J. Majer, A. Blais, M. H. Devoret, S. M. Girvin, and R. J. Schoelkopf, Phys. Rev. A **76**, 042319 (2007).
[79] A. Blais, J. Gambetta, A. Wallraff, D. I. Schuster, S. M. Girvin, M. H. Devoret, and R. J. Schoelkopf, Phys. Rev. A **75**, 032329 (2007).